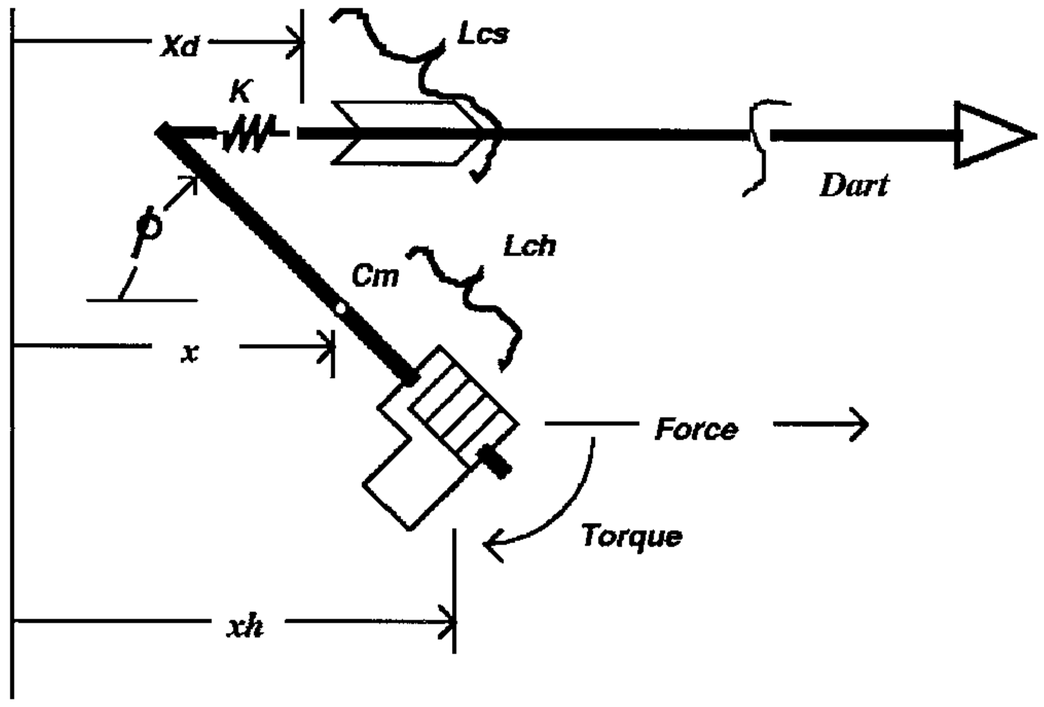

Fig. 5. The addition of a massless spring between the atlatl spur and the proximal end of the dart.

addition to the two original coordinates x and ϕ, a third, x_d, the horizontal position of the proximal end of the dart, is required. Then

$$KE=\tfrac{1}{2}(M_{ha}v_x^2+I_{ha}\omega^2+M_d v_d^2), \tag{7}$$

and the potential is

$$V=-\int_0^{x_h}F(u)du-\int_0^{\varphi}T(u)du + \tfrac{1}{2}k[x_d-(x-L_{cs}\cos(\phi))]^2. \tag{8}$$

We see that there are no terms in the kinetic energy involving the product of one velocity with another.

Initially x_h and $\phi=0$. The first term in Eq. (8) is integrated over the hand position, which is initially at C_m. The three equations of motion are then

$$M_{ha}\frac{d^2x}{dt^2}=F(x+L_{ch}\cos(\phi))+k[x_d-(x-L_{cs}\cos(\phi))] \tag{9}$$

for the center of mass,

$$I_{ha}\frac{d^2\phi}{dt^2}=T(x+L_{ch}\cos(\phi))-F(x+L_{ch}\cos(\phi)) \times L_{ch}\sin(\phi)-k(x-L_{cs}\cos(\phi)-xd)L_{cs}\sin(\phi) \tag{10}$$

for the atlatl rotation, and

$$M_d\frac{d^2x_d}{dt^2}=k(x-L_{cs}\cos(\phi)-x_d) \tag{11}$$

for the dart position.

An additional advantage of adding the spring is that it facilitates the analysis of flexibility in the atlatl. A rigid atlatl is represented by a large spring constant and a more flexible atlatl by a smaller spring constant. The Runge–Kutta differential equation solver in Mathcad readily solves these equations. As a check, the parameters of the system used in the experiment (Table I) were entered in the model. Figure 6 shows the horizontal velocity of the distal end of the spring versus time as measured and as computed from the model.

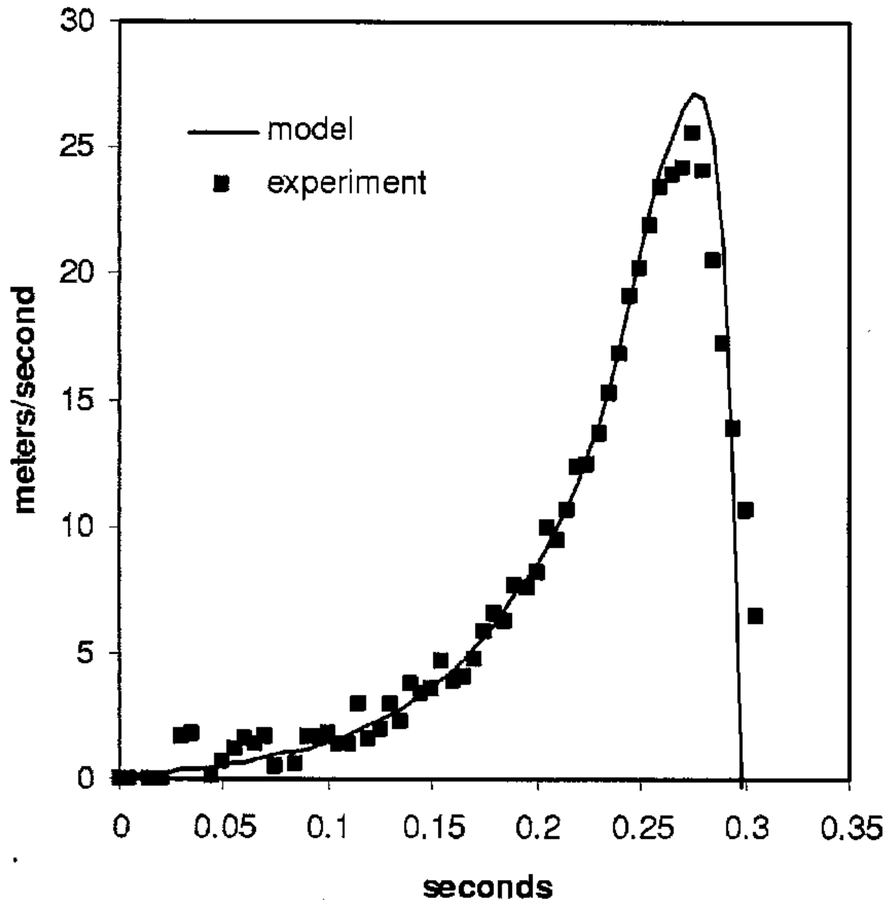

Fig. 6. Atlatl spur horizontal velocity. Experiment (■) and model (solid line).

The dart separates from the spring immediately after the maximum velocity occurs and continues on with that velocity.

VI. RESULTS OF COMPUTER MODEL

The objectives of the model are to quantify the relationship between dart velocity, dart mass, and atlatl dimensions and to analyze the effect of flexibility in the atlatl. The selection of the atlatl and dart dimensions to use in the model is determined by the archaeological and ethnographic records and by the practice of contemporary users of the atlatl. In Ref. 8, 33 hand thrown spears and 293 atlatl darts from Australia were examined, but the dimensions of the atlatls used with the darts were not mentioned. The mean mass of the hand thrown spears was 740 g with a fairly uniform distribution from 100 to 1350 g. The darts had a mean mass of 246 g with a range of 50 to 850 g; a fraction $\frac{58}{293}$ had masses between 50 and 100 g. Reference 9 discusses examples of Australian spear throwers ranging from 0.51 to 1.17 m long and Inuit (Eskimo) spear throwers about 0.50 m long. A Great Basin atlatl dart with a mass of 57 g has been replicated and Great Basin atlatls lengths ranging from 0.45 to 0.71 m have been cited.[10] The 7 darts considered in Ref. 4 ranged from 52 to 91 g with a mean of 73, the atlatls ranged from 0.48 to 0.57 m long with a weight from 72 to 82 g, and an added weight of 40 g. The dimensions of an atlatl and dart manufactured by BPS Engineering are cited in Table I.[11] We did calculations for 50, 73, 150, and 250 g darts as representative of the lighter Aboriginal darts, the BPS dart, and replicas in Refs. 4 and 10. The different atlatls used in the initial model are rigid and have mass proportional to length: $M_a=0.082L_a/0.61=0.134$ kg/m. The quantities L_{ch}, I_{ch}, and M_a, the distance from center of mass to hand, moment of inertia, and atlatl mass as a function of atlatl length, are defined in the Appendix.

The data is summarized in Fig. 7. Surprisingly, the simulation implies that the atlatl length for maximum velocity is much shorter than what is observed in actual practice. There could be several reasons for this. The initial assumption that the human effort (force and torque) is independent of the